



HAL
open science

Hydroxyl and sulfate radical-based oxidation of RhB dye in UV/H₂O₂ and UV/persulfate systems: Kinetics, mechanisms, and comparison

Xinxin Ding, Leonardo Gutierrez, Jean-Philippe Croué, Minrui Li, Lijun Wang, Yuru Wang

► To cite this version:

Xinxin Ding, Leonardo Gutierrez, Jean-Philippe Croué, Minrui Li, Lijun Wang, et al.. Hydroxyl and sulfate radical-based oxidation of RhB dye in UV/H₂O₂ and UV/persulfate systems: Kinetics, mechanisms, and comparison. *Chemosphere*, 2020, 253, pp.126655. 10.1016/j.chemosphere.2020.126655 . hal-03490270

HAL Id: hal-03490270

<https://hal.science/hal-03490270>

Submitted on 20 May 2022

HAL is a multi-disciplinary open access archive for the deposit and dissemination of scientific research documents, whether they are published or not. The documents may come from teaching and research institutions in France or abroad, or from public or private research centers.

L'archive ouverte pluridisciplinaire **HAL**, est destinée au dépôt et à la diffusion de documents scientifiques de niveau recherche, publiés ou non, émanant des établissements d'enseignement et de recherche français ou étrangers, des laboratoires publics ou privés.



Distributed under a Creative Commons Attribution - NonCommercial 4.0 International License

1 **Hydroxyl and sulfate radical-based oxidation of RhB dye in UV/H₂O₂ and**
2 **UV/persulfate systems: kinetics, mechanisms, and comparison**

3

4

5 Xinxin Ding ^a, Leonardo Gutierrez ^b, Jean-Philippe Croue ^{c*},

6

7 Minrui Li ^a, Lijun Wang ^a, Yuru Wang ^{a*}

8 ^aDepartment of Environmental Science, School of Geography and Tourism, Shaanxi

9 Normal University, Xi'an 710119, China

10 ^bFacultad del Mar y Medio Ambiente, Universidad del Pacifico, Ecuador

11 ^cInstitut de Chimie des Milieux et des Matériaux IC2MP UMR 7285 CNRS,

12 Université de Poitiers, France

13

14 *: Corresponding authors

15 E-mail address: jean.philippe.croue@univ-poitiers.fr; wangyuru@snnu.edu.cn

16

17

18

19 **Abstract**

20 The degradation kinetics and mechanisms of Rhodamine B (RhB) dye by $\cdot\text{OH}$ and $\text{SO}_4\cdot^-$ based
21 advanced oxidation processes were investigated. The $\cdot\text{OH}$ and $\text{SO}_4\cdot^-$ radicals were generated by
22 UV photolysis of hydrogen peroxide and persulfate (i.e., UV/H₂O₂ and UV/PS), respectively. The
23 effects of initial solution pH, RhB concentration, oxidant dosage, Fe²⁺ concentration, and water
24 matrices were examined. The results showed that the degradation of RhB followed
25 pseudo-first-order kinetics in both processes, with the UV/H₂O₂ process exhibiting better
26 performance than that of the UV/PS process. Acidic conditions were favorable to the degradation
27 of RhB in both systems. Increasing the oxidant dosage or decreasing the contaminant
28 concentration could enhance the degradation of RhB. Photo-Fenton-like processes accelerated the
29 performance when Fe²⁺ was added into both systems. The removal efficiency of RhB was
30 inhibited upon the addition of Humic Substances. The addition of Cl⁻ displayed no significant
31 effect and promoted RhB degradation in UV/H₂O₂ and UV/PS systems, respectively. The presence
32 of NO₃⁻ promoted RhB degradation, while H₂PO₄⁻ and C₂O₄²⁻ showed an inhibitory effect on both
33 UV/H₂O₂ and UV/PS processes. Radical scavenging tests revealed the dominant role of $\text{SO}_4\cdot^-$
34 radicals in the UV/PS system. Furthermore, the evolution of low molecular weight organic acids
35 and NH₄⁺ during the degradation of RhB in these two processes were compared. Both UV/H₂O₂
36 and UV/PS systems led to similar formation trends of NH₄⁺ and some ring-opening products (e.g.,
37 formic acid, acetic acid, and oxalic acid), suggesting some analogies in the decay pathways of
38 RhB by $\cdot\text{OH}$ and $\text{SO}_4\cdot^-$ -induced oxidation processes.

39

40 **Keywords:** Hydroxyl radical, Sulfate radical, UV/H₂O₂, UV/PS, Rhodamine B

41

42 **1. Introduction**

43 Dyes are mainly aromatic and heterocyclic compounds with stable structures incorporating
44 color-display and polar groups, widely used in textile, plastic, cosmetics, medicine, food, and
45 other industries (GilPavas et al., 2019). Briefly, more than 1.28×10^6 tons of commercial dyes were
46 produced world-wide in 2018 (Zhou et al., 2019). Remarkably, approximately 5-15% of the dyes
47 are released into the environment during their production and dyeing processes; thus, leading to
48 the generation of wastewater with dye concentrations varying from 5 to 1500 mg/L (Dong et al.,
49 2010; Kim et al., 2015). These organic pollutants can disrupt photosynthesis, inhibit the growth of
50 aquatic biota, and pose considerable health risks to human skin, eyes, gastrointestinal, and
51 respiratory systems (Dong et al., 2010; Wang and Chu, 2011; Su et al., 2013). Consequently,
52 dye-containing effluents discharged into the environment without proper treatment can have major
53 negative impacts on both aquatic ecosystems and human health. Besides, dyes are generally
54 resistant to light, aerobic digestion, and other conventional treatment processes due to their
55 complex structures (Xu and Li, 2010; GilPavas et al., 2019; Masi et al., 2019). Therefore, the
56 development of efficient and economical technologies for the degradation of dye contaminants
57 from wastewater before discharge is of critical importance.

58 Recently, UV-based Advanced Oxidation Processes (AOPs) have drawn increasing scientific
59 attention for degrading various types of refractory organic pollutants in water (Wang et al., 2017;
60 Nihemaiti et al., 2018; Liu et al., 2020). Particularly, the UV/H₂O₂ process is an attractive option
61 for the production of non-selective and highly reactive $\cdot\text{OH}$ radical ($E_0 = 1.8 - 2.7 \text{ V}$), which
62 displays a second-order rate constant with numerous contaminants at a near diffusion-controlled

63 rate ($k=10^{10} \text{ M}^{-1}\text{S}^{-1}$) (Buxton et al., 1988; Keen and Linden, 2013). Besides, persulfate (PS) has
64 also emerged as an alternative oxidant due to its capacity to generate sulfate radical ($\text{SO}_4^{\bullet-}$) under
65 UV irradiation (i.e., UV/PS). $\text{SO}_4^{\bullet-}$ is a strong oxidant ($E_0 = 2.5 - 3.1 \text{ V}$) with an oxidizing ability
66 comparable to $\bullet\text{OH}$; however, showing higher selectivity and longer half-life than $\bullet\text{OH}$ (Neta et al.,
67 1988; Rao et al., 2019). Compared to H_2O_2 , the advantages of persulfate as a radical
68 precursor include: relative stability in solid-state, high aqueous solubility, and high stability at
69 ambient environments, which facilitate its transport, storage, and usage (Zhang et al., 2014).
70 Therefore, $\text{SO}_4^{\bullet-}$ has also been increasingly tested in the removal of bio-recalcitrant organic
71 pollutants (Zhang et al., 2013; Khan et al., 2017). Both UV/ H_2O_2 and UV/PS processes have
72 demonstrated their effectiveness at degrading a wide range of organic pollutants, including
73 antibiotics, iodinated X-rays contrast media, and other PPCPs (Nihemaiti et al., 2018; Zhao et al.,
74 2019; Liu et al., 2020).

75 Rhodamine B (RhB) is a water-soluble xanthene dye mainly used as an additive in food stuffs;
76 however, it was banned in many countries due to its toxicity and carcinogenicity. The toxicity of
77 RhB has been well documented in the literature (Nestmann et al., 1979). Nevertheless, RhB is still
78 extensively applied as a colorant in textile dyeing, resulting in the production of large amounts of
79 RhB-containing effluents. Due to its high solubility and color rendering, water containing RhB,
80 even at low concentrations, can significantly impact the quality of surface water and disrupt the
81 photosynthesis of aquatic organisms (Su et al., 2013). Various UV-based AOPs have been
82 investigated for the effectiveness of RhB degradation. Zhang et al. (2020) reported that
83 approximately 90% of RhB removal was obtained in a UV enhanced electro-Fenton process where
84 $\bullet\text{OH}$ radical was found as the dominant radical species. Chen et al. (2012) revealed the good

85 degradation efficiency of RhB dye in a $\text{SO}_4^{\bullet-}$ -based UV/PS process and evaluated the influence of
86 some factors (e.g., oxidant dose and water matrix) on the degradation kinetics. Previous studies
87 indicated that the UV/PS process degraded organics more efficiently in buffered pure water than
88 that of the UV/ H_2O_2 process, while the process performance was significantly reduced when
89 applied to wastewater effluent due to the higher sensitivity and selectivity of $\text{SO}_4^{\bullet-}$ radical toward
90 water matrix and organics compared with $\cdot\text{OH}$ radical (Nihemaiti et al., 2018), suggesting the
91 significant role of water matrix and compound property on the performance of these two
92 UV-AOPs. However, to the best of our knowledge, there are no previous studies systematically
93 comparing hydroxyl and sulfate radical-based AOPs for the removal of RhB dye in water. Besides,
94 the decay pathways regarding the aromatic intermediates during the degradation of RhB by
95 hydroxyl and sulfate radical oxidation have been proposed in previous studies (He et al., 2009; Hu
96 et al., 2017; Rasheed et al., 2018). Nevertheless, limited information is available focusing on the
97 evolution of low molecular weight (LMW) carboxylic acids upon the ring-opening of aromatic
98 byproducts of RhB, which are usually more refractory towards further mineralization.

99 Therefore, the efficiency and degradation kinetics of UV/ H_2O_2 and UV/PS processes to
100 degrade RhB in synthetic wastewater were investigated and compared in this study. The influence
101 of some important experimental parameters (e.g., initial solution pH, oxidant dosage, and the
102 presence of oxidant activator) and solution chemistry (e.g., inorganic ions and dissolved organic
103 matter) on the efficiency of these oxidation processes was evaluated. Radical scavenging
104 experiments were conducted to identify the dominant radical species responsible for the RhB
105 decay. Furthermore, the evolution of some LMW organic intermediates (e.g., carboxylic acids)
106 and inorganic ions produced upon the degradation of RhB was examined, and the possible

107 degradation mechanism was accordingly proposed. The current investigation will highly assist in
108 better understanding the oxidation of RhB by UV/H₂O₂ and UV/PS processes for the successful
109 implementation of these technologies in the treatment of dye-contaminated wastewaters.

110 **2. Materials and methods**

111 *2.1. Chemical reagents*

112 All chemical reagents were of analytical grade and used as received without further
113 purification. Potassium persulfate (K₂S₂O₈, >99%), methanol (CH₃OH, 99.9%), and tert-butanol
114 (C₄H₁₀O, 99%) were purchased from Sigma-Aldrich. Rhodamine B (C₂₈H₃₁ClN₂O₃), hydrogen
115 peroxide (H₂O₂, 30%), nitrobenzene (NB), benzoic acid (BA), sodium thiosulfate (Na₂S₂O₃),
116 potassium chloride (KCl), ferrous sulfate heptahydrate (Fe₂SO₄·7H₂O), sodium oxalate (C₂Na₂O₄,
117 99.8%), potassium dihydrogen phosphate (K₂HPO₄), and sodium nitrate (NaNO₃) were provided
118 by Sinopharm Chemical Reagent Co., Ltd. (China). The humic substances (hydrophobic acid
119 fraction, i.e., DOM adsorbed onto XAD-8[®] resin at acid pH and recovered by caustic desorption)
120 used in this study were previously extracted from Suwannee River water (USA). Ultrapure water
121 (conductivity of 18.25 M Ω·cm) used in the experiments was obtained from the Cascada[™]
122 BIO water purification system (Pall Corporation, United Kingdom).

123 *2.2. Experimental procedures*

124 The irradiation experiments were performed in quartz tubes under continuous stirring and
125 temperature control (20±2°C) with a photochemical reaction apparatus (BL-GHX-V, Shanghai
126 Bilang Instrument Co., Ltd., China), equipped with a 300 W medium-pressure ultraviolet mercury
127 lamp ($\lambda_{\max} = 365$ nm) provided by the same manufacturer as the UV light source. Eight tubular
128 quartz reactors were evenly distributed in a circle centered around the lamp with a radius of 9.5

129 cm. The schematic illustration of the experimental setup and the irradiation spectrum of the light
130 source are provided in [Figs. S1 and S2](#) in the Supplementary Information (SI), respectively. The
131 average UV fluence rate (E_p^0) entering the solution was determined as 2.67 mW/cm^2 by
132 iodide/iodate chemical actinometry ([Bolton et al., 2011](#)). The final applied fluence was 2060
133 mJ/cm^2 , unless otherwise stated. The photochemical reactor and temperature control system were
134 turned on at least 20 min in advance to ensure stable conditions at the start of the experiments.

135 The degradation kinetics of RhB in the UV/H₂O₂ or UV/PS process were investigated by
136 sequentially spiking a specific amount of RhB, H₂O₂, or PS stock solution in ultrapure water. The
137 initial pH of the solution was adjusted with sulfuric acid (0.1 M) and sodium hydroxide (0.1 M).
138 No buffer solution was used in this study to avoid potential reactions between the radicals and
139 buffer solution. The reaction was initiated by adding a specific amount of H₂O₂ or PS into the
140 aqueous solution containing the probe contaminant while simultaneously subjected to UV
141 irradiation. The reaction volume of the solutions was set at 50 mL. The samples were collected at
142 predetermined time intervals and immediately quenched by adding sodium thiosulfate in excess.
143 There is some uncertainty in the literature regarding the effectiveness of sulfur-based reductants
144 (e.g., bisulfite and thiosulfate) as a quencher of H₂O₂ as reported by [Wang et al. \(2019\)](#).
145 Nevertheless, preliminary experiments conducted at pH from 2 to 11 demonstrated the
146 insignificance of H₂O₂ or PS alone for the RhB degradation ([Fig. S3](#)). Thus, the potential effect of
147 any residual oxidant on the decay result of RhB should be negligible. The collected samples were
148 filtered through a $0.45 \text{ }\mu\text{m}$ membrane before analysis with High-Performance Liquid
149 Chromatography (HPLC).

150 *2.3. Analytical methods*

151 The residual concentrations of RhB, NB, and BA were determined using a Dianex UltiMate
152 3000 HPLC system measuring the absorbance at 554, 270, and 230 nm, respectively. The
153 separation was performed on a Pinnacle II C18 column (250 mm × 4.6 mm with i.d. of 5 μm,
154 Restek). The mobile phase consisted of 60% acetonitrile and 40% water (V/V), while the flow rate
155 was set at 1.0 mL/min. The separation of LMW organic acids and ammonia was conducted by a
156 Dionex IC-1500 Ion Chromatography interfaced with a Dionex DS6 Conductivity Detector. A
157 Dionex IonPac AS19 column (4 mm × 250 mm) with its respective guard column (IonPac AG19,
158 4 mm × 50 mm) was used for the separation of LMW organic acids with a KOH gradient elution
159 (conditioning: 5 min at 1 mM; elution: 28 min at 18 mM to 35 mM, rinsing: 5 min at 1 mM) at a
160 flow rate of 1.0 mL/min. For ammonia analysis, a Dionex IonPac CG12A guard column (4 mm ×
161 50 mm) connected to an IonPac CS12A analytical column (4 mm × 250 mm) was used; while
162 eluted by 20 mM methanesulfonic acid at a flow rate of 1.0 mL/min. The Total Organic Carbon
163 (TOC) content of the samples was determined using a TOC-LCPH analyzer (Shimadzu, Japan)
164 through catalytic combustion oxidation at 680°C and analysis with a non-dispersive infrared
165 detector.

166 **3. Results and discussion**

167 *3.1. RhB degradation kinetics in different oxidation systems*

168 The degradation of RhB in different oxidation systems including H₂O₂ alone, PS alone, UV
169 irradiation, UV/H₂O₂, and UV/PS at neutral solution pH was investigated and compared. The
170 degradation of RhB by H₂O₂ or PS alone was negligible, indicating that in the absence of
171 activation these two oxidants are ineffective toward RhB at neutral pH (Fig.1). Under
172 UV irradiation, the removal of RhB reached 45% after 6 minutes of exposure. An enhanced

173 degradation was observed when UV irradiation was conducted in the presence of H₂O₂ or PS due
174 to the expected generation of [•]OH and/or SO₄^{•-} radicals. Remarkably, UV/H₂O₂ was more efficient
175 than UV/PS for the removal of RhB. Only 2 minutes and 4 minutes of irradiation were necessary
176 to decrease the concentration of RhB by 50% for UV/H₂O₂ and UV/PS process, respectively (Fig.
177 1a). After 15 min, approximately 96% and 87% of RhB were removed by the UV/H₂O₂ and
178 UV/PS processes, respectively. The reactions followed pseudo-first-order kinetics (R²>0.97) (Fig.
179 1b) The experimental rate constants (*k*_{obs}) derived from the slope of ln(C/C₀) versus time were
180 0.080, 0.150, and 0.219 min⁻¹ for UV, UV/PS, and UV/H₂O₂, respectively.

181 3.2. Effect of initial solution pH on the degradation kinetics

182 The influence of initial solution pH ranging from 2 to 11 on RhB degradation in UV/H₂O₂
183 and UV/PS systems was investigated (Fig. S4, SI). For all pH conditions, the reaction in the two
184 systems followed pseudo-first-order kinetics (R²>0.98). The decay rate constant (*k*_{obs}) of RhB in
185 both UV-based AOP systems significantly decreased with increasing pH (i.e., from pH 2 to 7);
186 however, *k*_{obs} remained approximately constant from pH 7 to 11 (Fig. 2).

187 This general pH trend on the degradation of RhB by AOPs was previously observed by others,
188 i.e., UV/H₂O₂ (Daneshvar et al., 2008), UV/S₂O₈²⁻ (Chen et al., 2012), Ozone/H₂O₂ (Bai et al.,
189 2011). The decrease in the process efficiency with increasing pH was also demonstrated for other
190 molecules e.g., ofloxacin, levofloxacin, and thiamphenicol with UV/H₂O₂ or UV/PS (Wang et al.,
191 2017; Liu et al., 2020). All these studies attributed this result, to a large extent, to the higher
192 production of radicals under acidic pH conditions and the scavenging and competing reactions
193 occurring at more alkaline pH. The role of hydroxyl ions in the complex propagation and
194 termination radical reaction mechanisms influencing the stability and reactivity of the produced

195 radical species have been well described in the above-listed publications and review articles (Stefan,
196 2017). The competing reactions with the formed by-products and the radical scavenging effect of
197 carbonate species (bicarbonate and carbonate ions) at neutral and alkaline pHs produced from the
198 degradation of the target compound (Criquet and Leitner, 2009) or possibly introduced from
199 enhanced dissolution from atmospheric CO₂ are also of significant importance (Baeza and Knappe,
200 2011). The impact of carbonate species on the performance of UV/H₂O₂ and UV/PS treatment
201 processes for contaminant degradation has been well documented (Wang et al., 2017; Nihemaiti et
202 al., 2018).

203 It is also accepted that the change in molar absorptivity and quantum yield with the pH of the
204 targeted compound can have a significant impact on the pseudo-first-order rate constant (Shen and
205 Lin, 2003). Baeza and Knappe (2011) have noted that the impact of the pH on the UV/H₂O₂ AOP
206 efficiency varied depending on the presence of either the neutral or the charged form (anionic or
207 cationic) of the molecule (i.e., as a function of pK_a), which significantly influenced the direct
208 photolysis rate constant but had little effect on the hydroxyl radical oxidation rate. RhB is
209 characterized by a pK_a value of 3.1 (Arbeloa and Ojeda, 1982) or 3.7 (Wang et al., 2014).
210 Increasing the pH from 2 to 4 implies a change in the molecular conformation of RhB from its
211 cationic form to its neutral/zwitterion form, a change that can possibly influence the degradation
212 efficiency of both AOPs. The direct photolysis rate of RhB ($k = 0.080 \text{ min}^{-1}$ at pH 7), which
213 contributes to a large part of the degradation of the molecule, should not differ above pH 4. No
214 significant change of the k_{obs} was noted from pH 7 to 11, which suggests a relatively constant
215 contribution of the radical species to the degradation of RhB.

216 Results depicted in Fig.2 showed similar k_{obs} of RhB for the two AOPs at acid pH (pH<7) and
217 high alkaline pH (pH 11). This similarity was not observed in the previous referred studies. At acid
218 pH, $\cdot\text{OH}$ and $\text{SO}_4^{\cdot-}$ radicals are predominant in the UV/H₂O₂ and UV/PS treatment processes,
219 respectively. At very high pH 11, the reaction between $\text{SO}_4^{\cdot-}$ and OH^- becomes significant,
220 converting most of $\text{SO}_4^{\cdot-}$ radicals to $\cdot\text{OH}$ radicals (Fang et al., 2012). At pH 11, the RhB solution
221 was subjected to $\cdot\text{OH}$ radical attack only in both AOP conditions. At a solution pH ranging from 7
222 to 9, $\text{SO}_4^{\cdot-}$ and $\cdot\text{OH}$ radicals were simultaneously present in the system; for this pH condition the
223 pseudo-first-order rate constant determined under UV/H₂O₂ treatment was systematically higher
224 than the one obtained for the UV/PS process. The nature and/or the relative abundance of the
225 formed by-products in this pH range may differ from the two AOPs and control the degradation
226 rate of RhB.

227 3.3. Effect of the initial RhB concentration and oxidant dose

228 The degradation efficiency of RhB at pH 7 decreased with increasing initial RhB
229 concentration in both UV/H₂O₂ and UV/PS systems after 15 min reaction time (Fig.3a). At
230 concentrations of 2.5, 5, 10, and 20 μM , the degradation efficiencies in the UV/H₂O₂ system were
231 98.8%, 98.7%, 95.6%, and 65.3%; and 100%, 98.3%, 86.7%, and 59.0% in the UV/PS system,
232 respectively. In the UV/H₂O₂ system, the pseudo-first-order reaction constant k_{obs} ($R^2 > 0.98$)
233 gradually decreased from 0.555 to 0.106 min^{-1} as the RhB concentration increased from 2.5 to 20
234 μM ; while in the UV/PS system, the k_{obs} decreased from 0.841 to 0.085 min^{-1} , respectively. The
235 decrease of k_{obs} with increasing RhB concentration can be explained as follows.

236 Firstly, RhB exhibits two main absorption peaks at 259 nm and 554 nm. The absorption of
237 RhB at the UV region can hinder the efficiency of the UV-based AOPs by reducing the amount of

238 applied fluence. In this study, an increase in RhB concentration from 2.5 to 20 μM led to an
239 increase of UV absorbance at 254 and 365 nm from 0.165 to 0.497 and 0.066 to 0.163,
240 respectively, which significantly enhanced its inner filter effect and resulted in a decrease in the
241 corresponding applied fluence by 38.9% and 15.1%, respectively. Consequently, the available UV
242 fluence for activating H_2O_2 and PS for $\cdot\text{OH}$ and $\text{SO}_4^{\cdot-}$ production was remarkably reduced; thus,
243 decreasing the amount of $\cdot\text{OH}$ and/or $\text{SO}_4^{\cdot-}$ available to react with the target compound. Secondly,
244 the byproducts generated in solution at high RhB dose also compete with their mother compound
245 for $\cdot\text{OH}$ and $\text{SO}_4^{\cdot-}$ consumption and in turn decrease the overall RhB decay (Wang and Chu, 2011).
246 These results are consistent with previous observations by Rehman et al. (2018) and Isari et al.
247 (2018), indicating that the initial concentration of the contaminant is an important
248 factor affecting its degradation rate.

249 As the precursor of active radicals, the concentrations of H_2O_2 and PS play a decisive role in
250 the overall degradation efficiency of the UV/ H_2O_2 and UV/PS processes (Fig. S5, SI).
251 Experimental results showed that increasing the H_2O_2 concentration from 10 to 200 μM , led to a
252 considerable enhancement in the removal of RhB in the UV/ H_2O_2 system (i.e., from 63% to
253 almost 99% after 10 min treatment), resulting in a significant increase in the corresponding decay
254 rate constant (i.e., from 0.101 to 0.408 min^{-1} in Fig. 3b). Similar results were obtained with the
255 UV/PS system. However, a large excess of H_2O_2 might induce enhanced scavenging effect by
256 reacting with $\cdot\text{OH}$ to produce less reactive species (conditions not studied in the current research),
257 which in turn would decrease the degradation rate of the target contaminant (Eqs. 1 and 2)
258 (Christensen et al., 1982; Pouran et al., 2015; Wang et al., 2017; Tian et al., 2019). Similarly, an
259 over-dosage of PS in the system can also inhibit the process efficiency because the side reactions

260 between PS and the generated $\text{SO}_4^{\bullet-}/\text{OH}^{\bullet}$ radicals to generate $\text{S}_2\text{O}_8^{\bullet-}$ (Eqs. 3 and 4) become more
261 substantial, while $\text{S}_2\text{O}_8^{\bullet-}$ is less reactive than $\text{SO}_4^{\bullet-}$; thus, inducing a quenching effect (Liang and
262 Su, 2009).



263 3.4. The multi-role of Fe^{2+} as an oxidant activator

264 The influence of Fe^{2+} as a transition metal activator of H_2O_2 and PS on the degradation of
265 RhB in H_2O_2 , PS, UV/ H_2O_2 , and UV/PS systems was investigated (Fig. S6, SI). The initial
266 solution pH was adjusted as 3 to avoid the oxidation of Fe^{2+} into Fe^{3+} and its subsequent
267 precipitation. The calculated k_{obs} increased with increasing Fe^{2+} concentration for all conditions
268 studied (Fig. 4). The addition of 100 μM Fe^{2+} as the activator of H_2O_2 (i.e., Fenton reagent) and
269 PS (i.e., Fenton-like reagent), increased the k_{obs} from 0 to 0.215 min^{-1} and 0.072 min^{-1} , respectively.
270 The efficiency of Fenton and Fenton-like reagents for the degradation of organic contaminants has
271 been previously well described in the literature (Chamarro et al., 2001; Xu and Li, 2010).

272 In the UV/ H_2O_2 system, the addition of 100 μM Fe^{2+} (i.e., causing the formation of a
273 photo-Fenton system) led to an increase in the removal of RhB from 78.1% to 99.4% in 3 min;
274 whereby the decay rate constant significantly increased by 4-fold (i.e., from 0.421 to 1.699 min^{-1}).
275 Compared to the UV/ H_2O_2 process, the substantial improvement in the process efficiency as a
276 result of the formation photo-Fenton system can be attributed to the additional production of OH^{\bullet}
277 radicals in two ways. One way involves the favorable OH^{\bullet} radical generation by the Fe^{2+} -activated

278 decomposition of H₂O₂ (Eq. 5). Another way providing an additional formation of •OH radicals is
 279 due to the photoreduction of hydroxylated Fe³⁺ ions or ferrihydroxalate (Fe(OH)²⁺) (Eq. 6), which
 280 can simultaneously regenerate Fe²⁺ ions and in turn further promote the process performance
 281 (Pouran et al., 2015). For the UV/PS system, when the concentration of Fe²⁺ in solution was
 282 increased to 100 μM, the target pollutant was almost completely degraded (>99%) within 3 min,
 283 while the RhB removal in the UV/PS process without Fe²⁺ ions was only 71%. Accordingly,
 284 the decay rate constant *k*_{obs} significantly increased from 0.366 to 1.617 min⁻¹ as dosing Fe²⁺ ions
 285 from 0 to 100 μM into the system. This result indicated that the addition of Fe²⁺ to the
 286 UV/PS system remarkably enhanced the degradation efficiency of contaminants by developing
 287 a Photo-Fenton-like oxidation system. Briefly, Fe²⁺ reacted with S₂O₈²⁻ to produce more SO₄^{•-} in
 288 the UV/PS system (Eq. 7) (Liang et al., 2008). Subsequently, the formed Fe³⁺ ions led to the
 289 generation of Fe(OH)²⁺ which further photolyzed into •OH radicals and Fe²⁺
 290 ions; thus, accelerating the degradation of RhB (Liang et al., 2008). Compared to the
 291 traditional Fenton reaction or the UV activated H₂O₂ or PS system,
 292 the Photo-Fenton-like oxidation system could significantly improve the degradation efficiency of
 293 pollutants.

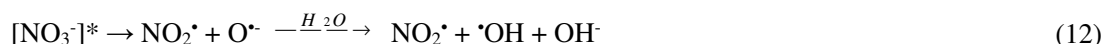


294 3.5. Effect of the water matrix on the degradation of RhB

295 Cl⁻, H₂PO₄⁻, NO₃⁻, and C₂O₄²⁻ are ubiquitously present in natural water and wastewaters. They
 296 can exert varying influence on the UV-based AOPs by either acting as a radical scavenger or

297 inducing photochemical effect. Thus, the RhB degradation in the presence of Cl^- , H_2PO_4^- , $\text{C}_2\text{O}_4^{2-}$,
298 or NO_3^- in both UV/ H_2O_2 and UV/PS systems was investigated and compared (Fig. 5a-c). The
299 concentration of chloride in natural water systems varies from around 1 to several mM. In some
300 surface waters, it may reach > 20 mM (Magazinovic et al., 2004). Accordingly, 10 mM chloride
301 was selected to investigate the effect of chloride on the process performance, while the impact of
302 other ions was conducted under the same conditions for comparison. The addition of
303 Cl^- exerted negligible impact on the UV/ H_2O_2 system, as predicted from by Eqs. 8 and 9 (Atinault
304 et al., 2008). There were some ClHO^\bullet formed by the reaction of Cl^- and $^\bullet\text{OH}$; however,
305 subsequently transformed back to $^\bullet\text{OH}$. Thus, the whole system was relatively stable. The addition
306 of Cl^- slightly accelerated the oxidation of RhB in the UV/PS system. A similar observation was
307 reported by Huang et al. (2017), who showed that above 5 mM, chloride ions improved the
308 degradation of RhB in a sulfate radical-based oxidation system. Nevertheless, an inhibitory effect
309 at a lower chloride dosage of 0-5 mM was observed. Generally, the presence of chloride ions
310 induces dual impact depending on the Cl^- concentration and the type of substrate. A low level, Cl^-
311 mainly leads to a scavenging effect by reacting with $\text{SO}_4^{\bullet-}$ to form less reactive chlorine radicals
312 (e.g., Cl^\bullet). Interestingly, the enhanced formation of reactive chlorine species (e.g., $\text{Cl}_2^{\bullet-}$ and HClO)
313 at higher chloride dosage can compensate the consumption of $\text{SO}_4^{\bullet-}$ and even increase the process
314 efficiency. When H_2PO_4^- and $\text{C}_2\text{O}_4^{2-}$ were introduced into the solution, the degradation of RhB
315 was negatively affected in both systems. This observation could be attributed to the formation of
316 $^\bullet\text{H}_2\text{PO}_4$ and $^\bullet\text{C}_2\text{O}_4^-$, which showed a relatively weak reactivity towards contaminants and a certain
317 quenching effect on $^\bullet\text{OH}$ and $\text{SO}_4^{\bullet-}$ radicals (Grgic et al., 2007; Xu and Li, 2010). Specifically, the
318 reactivity of $^\bullet\text{OH}$ and $\text{SO}_4^{\bullet-}$ with H_2PO_4^- was 2.0×10^4 and $7.2 \times 10^4 \text{ M}^{-1}\text{s}^{-1}$, respectively, while their

319 respective reaction rate constants with $C_2O_4^{2-}$ were $(5.3\pm 0.3)\times 10^6$ and $(1.3\pm 0.1)\times 10^7$ $M^{-1}s^{-1}$ (Getoff
320 et al., 1971; Neta et al., 1988; Grgic et al., 2007; Grebel et al., 2010). Thus, the performance of
321 both UV/H₂O₂ and UV/PS systems was significantly reduced by the addition of $C_2O_4^{2-}$ ions
322 compared to that of $H_2PO_4^-$ ions. Meanwhile, $C_2O_4^{2-}$ exhibited a stronger inhibition for the UV/PS
323 process than that of the UV/H₂O₂ process due to its higher reactivity towards sulfate radicals. RhB
324 removal efficiency was substantially increased in the presence of NO_3^- ions and the observed rate
325 constant of RhB decay in the UV/H₂O₂ and UV/PS systems was 1.6 and 2.2-fold of that control
326 tests (Fig. 5c), respectively. This significant performance enhancement resulted from the
327 formation of additional reactive species via the NO_3^- photolysis (Eqs. 10-12). The main pathway
328 of UV irradiation of NO_3^- ions yields hydroxyl radicals which benefit the process efficiency for
329 the UV-based AOPs (Shankar et al., 2007; Boucheloukh et al., 2012). Other studies have also
330 reported the promoting effect of NO_3^- ions on the UV-based systems (Rao et al., 2016). However,
331 NO_2^- formation by UV irradiation of NO_3^- might be of concern for nitrate-rich waters in the
332 present of DOM (Semitsoglou-Tsiapou et al., 2016).



333 Dissolved Organic Matter (DOM), such as Humic Substances (HS), is known to affect the
334 behavior of organic pollutants in the environment and engineering processes. It can induce a
335 significant influence on the performance of UV-based AOPs process by playing multiple roles.

336 The presence of highly reactive aromatic moieties within the DOM decreases the effective UV
337 fluence by acting as UV inner filter and consuming radical species (e.g., the rate constants of
338 $k_{\bullet\text{OH}/\text{NOM}}$ and $k_{\text{SO}_4^{\bullet-}/\text{NOM}}$ are 2.23×10^8 and $6.0 \times 10^6 \text{ M}^{-1}\text{s}^{-1}$, respectively) (Westerhoff et al., 2007;
339 Zhang et al., 2019); thus, ultimately inhibiting the degradation of contaminants. Therefore,
340 RhB degradation in UV/H₂O₂ and UV/PS systems was investigated in the presence of the
341 hydrophobic acid fraction isolated from the Suwannee River (HPOA-SWR). Fig. 5d illustrates the
342 pseudo-first-order kinetics of the reaction. The presence of HPOA-SWR significantly decreased
343 the k_{obs} of RhB decay in the two systems, displaying an exponential decrease in k_{obs}
344 with increasing HPOA-SWR concentration. Specifically, when the concentration
345 of DOM increased from 0 to 10 mg-C/L, the k_{obs} decreased by ~73% in both systems, and the
346 removal of RhB decreased from 95.6% to 54% and from 86.7% to 46% in UV/H₂O₂ and
347 UV/PS systems, respectively. The current experimental results demonstrated that the inhibitory
348 effect of background DOM in the water matrix should be of special concern for the UV-based
349 AOPs.

350 3.6. Predominant radicals in the oxidation systems

351 As common free radical scavengers, methanol (MeOH) can react with both $\bullet\text{OH}$ and $\text{SO}_4^{\bullet-}$
352 radicals at high rate constants ($k_{\bullet\text{OH}/\text{MeOH}} = 9.7 \times 10^8 \text{ M}^{-1}\text{s}^{-1}$ and $k_{\text{SO}_4^{\bullet-}/\text{MeOH}} = 1.1 \times 10^7 \text{ M}^{-1}\text{s}^{-1}$)
353 (Buxton et al., 1988; Neta et al., 1988); thus, effectively quenching these two radicals. Tert-butyl
354 alcohol (TBA) exhibited a higher reaction rate with $\bullet\text{OH}$ ($k_{\bullet\text{OH}/\text{TBA}} = (3.8\text{-}7.6) \times 10^8 \text{ M}^{-1}\text{s}^{-1}$), which
355 was considerably higher than that with $\text{SO}_4^{\bullet-}$ ($k_{\text{SO}_4^{\bullet-}/\text{TBA}} = (4.0\text{-}9.1) \times 10^5 \text{ M}^{-1}\text{s}^{-1}$) (Anipsitakis and
356 Dionysiou, 2004). Consequently, for processes involving the contribution of both $\bullet\text{OH}$ and $\text{SO}_4^{\bullet-}$
357 radicals, TBA could selectively capture $\bullet\text{OH}$ to inhibit the oxidation reaction and thereby the

358 specific role of $\cdot\text{OH}$ and $\text{SO}_4^{\cdot-}$ can be distinguished based on the different decay efficiencies. In the
359 UV/PS process, two main reactive radicals were generated: $\text{SO}_4^{\cdot-}$ and $\cdot\text{OH}$, both participating in
360 the reaction. To identify the predominant radicals in the UV/PS system, MeOH was
361 separately added to the solution at a ratio of 3000:1 and 1000:1 to oxidants, respectively. A similar
362 approach was conducted for TBA. Fig. 6 illustrates the comparative decay of the target
363 contaminant with and without radical scavengers in UV/ H_2O_2 and UV/PS systems.

364 Experimental results showed that both TBA and MeOH were effective $\cdot\text{OH}$ scavengers.
365 However, MeOH exhibited a higher scavenging capacity of radicals than TBA; thus, playing a
366 more important role in the inhibition of RhB decay. The degradation of RhB in
367 the UV/ H_2O_2 process—significantly decreased from 96% to 17% and 46% after adding 50 mM
368 MeOH and TBA (Fig. 6a), respectively. Increasing the concentration of TBA to 150 mM further
369 reduced the process efficiency by approximately 10%, while the addition of 150 mM MeOH led to
370 insignificant decrease in the RhB removal compared with that of 50 mM MeOH, suggesting that
371 $\cdot\text{OH}$ radicals generated in the UV/ H_2O_2 process were almost completely quenched by 50 mM
372 MeOH. Radical scavenging experiments in the UV/ H_2O_2 process indicated that $\cdot\text{OH}$
373 radicals contributed to almost 82% of RhB decay. In the UV/PS process, the addition of 50 mM
374 MeOH and TBA inhibited the process efficiency by 78% and 35.6%, respectively (Fig. 6b). The
375 remarkable difference between these two quenchers in the inhibitory effect on the RhB removal
376 suggested that both $\text{SO}_4^{\cdot-}$ and $\cdot\text{OH}$ radicals were involved in the degradation of RhB. Moreover,
377 the considerably more pronounced inhibition upon the addition of MeOH indicated the
378 predominant role of $\text{SO}_4^{\cdot-}$ radicals in the UV/PS process. When the molar ratio of MeOH or
379 TBA to PS increased from 1000:1 to 3000:1, the change in the removal of RhB was negligible.

380 This result confirmed that the system had relatively lower production of $\cdot\text{OH}$ and the low
381 concentration of quencher was sufficient. Based on the quenching experimental results, the
382 contribution of $\text{SO}_4^{\cdot-}$, $\cdot\text{OH}$, and direct photolysis to the degradation of RhB in the UV/PS process
383 was determined as 40%, 31%, and 16%, respectively. Moreover, this comparison found that the
384 two quenchers displayed a stronger inhibitory impact on the UV/ H_2O_2 system, indicating a higher
385 yield of $\cdot\text{OH}$ in this system.

386 To further investigate the production of reactive species in UV/ H_2O_2 and UV/PS systems, NB
387 and BA were used as radical probes. NB could selectively react with $\cdot\text{OH}$ following a second
388 order rate constant of $3.9 \times 10^9 \text{ M}^{-1}\text{S}^{-1}$, while BA reacts with both $\cdot\text{OH}$ and $\text{SO}_4^{\cdot-}$ with second order
389 rate constants of 5.9×10^9 and $1.2 \times 10^9 \text{ M}^{-1}\text{S}^{-1}$, respectively (Guan et al., 2011). The detailed
390 calculation of $\cdot\text{OH}$ and $\text{SO}_4^{\cdot-}$ can be found in [Text S1](#). The degradation of NB and BA in the tests
391 followed pseudo-first-order kinetics ($R^2 > 0.99$) ([Fig. 6c and 6d](#)). Hence, the steady-state
392 concentration of $\cdot\text{OH}$ was calculated as 4.04×10^{-13} and $2.73 \times 10^{-13} \text{ M}$ in UV/ H_2O_2 and UV/PS
393 systems, respectively. The concentration of $\text{SO}_4^{\cdot-}$ in the UV/PS system was $7.34 \times 10^{-13} \text{ M}$. These
394 results confirmed the predominant roles of $\cdot\text{OH}$ and $\text{SO}_4^{\cdot-}$ in UV/ H_2O_2 and UV/PS processes,
395 respectively.

396 *3.7. Intermediate identification and plausible mechanisms*

397 To explore the mechanism of RhB degradation in the UV/ H_2O_2 and UV/PS processes, the
398 initial concentration of oxidants and RhB was increased to a relatively higher concentration of 1
399 mM and 0.2 mM, respectively. Simultaneously, the TOC removal and the production of some
400 RhB decomposition intermediates (e.g., low molecular weight organic acids) were recorded by
401 TOC analyzer and IC ([Fig. 7](#)). After 4 h of treatment, the degradation efficiencies of the RhB in

402 both UV/H₂O₂ and UV/PS processes were almost 100% and the TOC removal was 50% and 60%,
403 respectively. During the degradation/decolorization of the RhB in both processes, a rapid
404 depletion in the two characteristic absorbance peaks (i.e., 259 nm at UV region and 554 nm at the
405 visible light region) of the RhB was observed (spectra shown in Fig. S7, SI), which corresponded
406 to the destruction of aromatic and the chromophore structures (i.e., C=N and C=O groups) (Jiang
407 et al., 2018), respectively. Meanwhile, five degradation intermediates were identified including
408 one inorganic ion (i.e., NH₄⁺) and four LMW organic acids, i.e., formate (HCOO⁻), acetate
409 (CH₃COO⁻), oxalate (C₂O₄²⁻), and lactate (C₃H₅O₃⁻). These small organic acids generally resulted
410 from the subsequent oxidation of longer-chain carboxylic acids, such as maleic and fumaric acids,
411 upon the benzene ring opening. Therefore, the degradation of RhB could be attributed to the
412 destruction of the conjugated groups and the N-de-ethylation upon attack by reactive radical
413 species like SO₄⁻ and [•]OH, causing the generation of some carboxylic acids by opening the
414 benzene rings, where the organic nitrogen could be oxidized to form NH₄⁺ after the N-position
415 de-ethylation in the molecules.

416 A first formation and then decay curve was observed for lactic acid (i.e., C₃H₅O₃⁻) in both
417 UV/H₂O₂ and UV/PS processes. The generation of C₃H₅O₃⁻ rapidly reached a maximum of
418 40.6 μM at 5 min in the UV/PS system, and then decreased. However, the yield of C₃H₅O₃⁻ in the
419 UV/H₂O₂ process was significantly lower with a peak concentration of 11.7 μM after 2 h. The
420 amount of all other small carboxylic acids showed an increasing formation trend as a function of
421 reaction time in both processes. Specifically, C₃H₅O₃⁻ was one of the intermediates formed before
422 RhB was mineralized into HCOO⁻ and CH₃COO⁻ (smaller molecular weight). The subsequent
423 decomposition of these intermediates upon further attack by radicals lead to a significant

424 accumulation of HCOO^- and CH_3COO^- in both UV/ H_2O_2 and UV/PS processes (Fig. 7). By
425 comparison, the yield of HCOO^- and CH_3COO^- in the UV/PS system was approximately 1.5-fold
426 higher than that in the UV/ H_2O_2 system. Meanwhile, a gradual accumulation of NH_4^+ ions was
427 recorded in both systems due to the oxidation of the N-de-ethylation. As subsequent oxidation
428 took place, NH_4^+ ions can be further converted into NO_3^- ions which were not detected in the
429 current study. The buildup of NH_4^+ ions after 4 h reached 26.3 and 52.8 μM in UV/ H_2O_2 and
430 UV/PS processes, respectively. The relatively higher transformation efficiency and more
431 production of end products in the UV/PS process indicated that at higher concentrations of both
432 contaminants and oxidants, the UV/PS process displayed a better performance and oxidability for
433 the RhB transformation.

434 **4. Conclusions**

435 In this study, UV light was used to activate H_2O_2 and PS to degrade the RhB dye in aqueous
436 solution through the formation of $\cdot\text{OH}$ and $\text{SO}_4^{\cdot-}$ radicals; whereby, the removal efficiency of
437 RhB in the two systems and under different conditions were compared. The results showed that:

438 (1) Both UV/ H_2O_2 and UV/PS processes displayed a good performance on the degradation of
439 RhB, and the decay followed pseudo-first-order kinetics. The removal of RhB decreased with
440 increasing pH, where the optimum pH value was 2 in both systems. In a certain range, the
441 degradation efficiency increased with increasing oxidant concentration and decreasing initial
442 concentration of RhB. The formation of photo-Fenton and photo-Fenton-like systems by
443 adding Fe^{2+} facilitated the oxidation performance. HS remarkably suppressed the process
444 efficiency by acting as UV inner filter and radical sink. The addition of Cl⁻ had no significant
445 impact on the UV/ H_2O_2 process; however, it slightly promoted the degradation in

446 the UV/PS system. The presence of NO_3^- substantially facilitated the oxidation of RhB in both
447 processes, while H_2PO_4^- and $\text{C}_2\text{O}_4^{2-}$ showed the opposite effect.

448 (2) Suppression tests by adding MeOH and TBA as radical scavengers and competition
449 kinetic tests by using NB and BA as relevant radical probes confirmed the dominant role of $\text{SO}_4^{\bullet-}$
450 radicals in the UV/PS process. The steady-state concentration of $\bullet\text{OH}$ was calculated as 4.04×10^{-13}
451 and 2.73×10^{-13} M in UV/ H_2O_2 and UV/PS systems, respectively, while the yield of $\text{SO}_4^{\bullet-}$ in the
452 UV/PS system was 7.34×10^{-13} M in the presence of 1 μM radical probes, 10 μM RhB, and 50 μM
453 oxidants at pH 7 in aqueous solution.

454 (3) The UV/PS process led to a relative higher TOC removal compared to that of the
455 UV/ H_2O_2 process in the current study. The transformation of RhB gave rise to the accumulation
456 of LMW carboxylic acids (e.g., formic acid, acetic acid, and oxalic acid) and the formation of
457 inorganic ions (i.e., NH_4^+). Accordingly, the degradation of RhB could be attributed to the opening
458 of the benzene rings and the oxidation of the organic nitrogen upon attack by $\text{SO}_4^{\bullet-}$ and $\bullet\text{OH}$
459 radical species, resulting in the generation of LMW carboxylic acids and NH_4^+ as transformation
460 products.

461 **Acknowledgments**

462 The research reported in this work was supported by the National Natural Science Foundation
463 of China (No.51508317), the Fundamental Research Funds for the Central Universities
464 (GK201802108), China Postdoctoral Science Foundation (No.2016M602762), and the Special
465 Financial Grant from the Shaanxi Postdoctoral Science Foundation (No.2017BSHTDZZ09).

466

467 **References**

- 468 Anipsitakis, G.P., Dionysiou, D.D., 2004. Radical generation by the interaction of transition metals
469 with common oxidants. *Environ. Sci. Technol.* 38, 3705-3712.
- 470 Arbeloa, I.L., Ojeda, P.R., 1982. Dimer states of Rhodamine B. *Chem. Phys. Lett.* 87, 556-560.
- 471 Atinault, E., De Waele, V., Schmidhammer, U., Fattahi, M., Mostafavi, M., 2008. Scavenging of e_s^- and
472 $OH\cdot$ radicals in concentrated HCl and NaCl aqueous solutions. *Chem. Phys. Lett.* 460, 461-465.
- 473 Baeza, C., Knappe, D.R.U., 2011. Transformation kinetics of biochemically active compounds in
474 low-pressure UV Photolysis and UV/H₂O₂ advanced oxidation processes. *Water Res.* 45,
475 4531-4543.
- 476 Bai, C.P., Xiong, X.F., Gong, W.Q., Feng, D.X., Xian, M., Ge, Z.X., Xu, N., 2011. Removal of
477 rhodamine B by ozone-based advanced oxidation process. *Desalination* 278, 84-90.
- 478 Bolton, J.R., Stefan, M.I., Shaw, P.-S., Lykke, K.R., 2011. Determination of the quantum yields of the
479 potassium ferrioxalate and potassium iodide-iodate actinometers and a method for the calibration
480 of radiometer detectors. *J. Photoch. Photobio. A* 222, 166-169.
- 481 Boucheloukh, H., Sehili, T., Kouachi, N., Djebbar, K., 2012. Kinetic and analytical study of the
482 photo-induced degradation of monuron by nitrates and nitrites under irradiation or in the dark.
483 *Photoch. Photobio. Sci.* 11, 1339-1345.
- 484 Buxton, G.V., Clive L, G., W, P.H., Alberta B, R., 1988. Critical Review of rate constants for reactions
485 of hydrated electrons, hydrogen atoms and hydroxyl radicals ($\cdot OH/O^-$ in Aqueous Solution. *J.*
486 *Phys. Chem. Ref. Data* 17, 513-886.
- 487 Chamarro, E., Marco, A., Esplugas, S., 2001. Use of Fenton reagent to improve organic chemical
488 biodegradability. *Water Res.* 35, 1047-1051.
- 489 Chen, X., Xue, Z., Yao, Y., Wang, W., Zhu, F., Hong, C., 2012. Oxidation Degradation of Rhodamine B
490 in Aqueous by UV/S₂O₈²⁻ Treatment System. *International Journal of Photoenergy*, 1-5.
- 491 Christensen, H., Sehested, K., Corfitzen, H., 1982. Reactions of hydroxyl radicals with hydrogen
492 peroxide at ambient and elevated temperatures. *J. Phys. Chem.* 86, 1588-1590.
- 493 Criquet, J., Leitner, N.K.V., 2009. Degradation of acetic acid with sulfate radical generated by
494 persulfate ions photolysis. *Chemosphere* 77, 194-200.
- 495 Daneshvar, N., Behnajady, M.A., Mohammadi, M.K.A., Dorraji, M.S.S., 2008. UV/H₂O₂ treatment of
496 Rhodamine B in aqueous solution: Influence of operational parameters and kinetic modeling.
497 *Desalination* 230, 16-26.
- 498 Dong, W.Y., Lee, C.W., Lu, X.C., Sun, Y.J., Hua, W.M., Zhuang, G.S., Zhang, S.C., Chen, J.M., Hou,
499 H.Q., Zhao, D.Y., 2010. Synchronous role of coupled adsorption and photocatalytic oxidation on
500 ordered mesoporous anatase TiO₂-SiO₂ nanocomposites generating excellent degradation activity
501 of RhB dye. *Appl. Catal. B Environ.* 95, 197-207.
- 502 Fang, G.-D., Dionysiou, D.D., Wang, Y., Al-Abed, S.R., Zhou, D.-M., 2012. Sulfate radical-based
503 degradation of polychlorinated biphenyls: Effects of chloride ion and reaction kinetics. *J. Hazard*
504 *Mater.* 227, 394-401.
- 505 Getoff, N., F. Schworer, V.M. Markovic, K. Sehested, Nielsen, S.O., 1971. Pulse radiolysis of oxalic
506 acid and oxalates. *J. Phys. Chem.* 75, 749-755.

507 GilPavas, E., Dobrosz-Gomez, I., Gomez-Garcia, M.-A., 2019. Optimization and toxicity assessment of
508 a combined electrocoagulation, $H_2O_2/Fe^{2+}/UV$ and activated carbon adsorption for textile
509 wastewater treatment. *Sci. Total Environ.* 651, 551-560.

510 Grebel, J.E., Pignatello, J.J., Mitch, W.A., 2010. Effect of Halide Ions and Carbonates on Organic
511 Contaminant Degradation by Hydroxyl Radical-Based Advanced Oxidation Processes in Saline
512 Waters. *Environ. Sci. Technol.* 44, 6822-6828.

513 Grgic, I., Podkrajsek, B., Barzaghi, P., Herrmann, H., 2007. Scavenging of SO_4^- radical anions by
514 mono- and dicarboxylic acids in the Mn(II)-catalyzed S(IV) oxidation in aqueous solution. *Atmos.*
515 *Environ.* 41, 9187-9194.

516 Guan, Y.-H., Ma, J., Li, X.-C., Fang, J.-Y., Chen, L.-W., 2011. Influence of pH on the Formation of
517 Sulfate and Hydroxyl Radicals in the UV/Peroxymonosulfate System. *Environ. Sci. Technol.* 45,
518 9308-9314.

519 He, Z., Sun, C., Yang, S., Ding, Y., He, H., Wang, Z., 2009. Photocatalytic degradation of rhodamine B
520 by Bi_2WO_6 with electron accepting agent under microwave irradiation: Mechanism and pathway.
521 *J. Hazard Mater.* 162, 1477-1486.

522 Hu, L., Deng, G., Lu, W., Lu, Y., Zhang, Y., 2017. Peroxymonosulfate activation by
523 Mn_3O_4 /metal-organic framework for degradation of refractory aqueous organic pollutant
524 rhodamine B. *Chinese Journal of Catalysis* 38, 1360-1372.

525 Huang, Y., Wang, Z., Liu, Q., Wang, X., Yuan, Z., Liu, J., 2017. Effects of chloride on PMS-based
526 pollutant degradation: A substantial discrepancy between dyes and their common decomposition
527 intermediate (phthalic acid). *Chemosphere* 187, 338-346.

528 Isari, A.A., Payan, A., Fattahi, M., Jorfi, S., Kakavandi, B., 2018. Photocatalytic degradation of
529 rhodamine B and real textile wastewater using Fe-doped TiO_2 anchored on reduced graphene
530 oxide ($Fe-TiO_2/rGO$): Characterization and feasibility, mechanism and pathway studies. *Appl.*
531 *Surf. Sci.* 462, 549-564.

532 Jiang, L., Zhang, Y., Zhou, M., Liang, L., Li, K., 2018. Oxidation of Rhodamine B by persulfate
533 activated with porous carbon aerogel through a non-radical mechanism. *J. Hazard Mater.* 358,
534 53-61.

535 Keen, O.S., Linden, K.G., 2013. Degradation of Antibiotic Activity during UV/H_2O_2 Advanced
536 Oxidation and Photolysis in Wastewater Effluent. *Environ. Sci. Technol.* 47, 13020-13030.

537 Khan, S., He, X., Khan, J.A., Khan, H.M., Boccelli, D.L., Dionysiou, D.D., 2017. Kinetics and
538 mechanism of sulfate radical- and hydroxyl radical-induced degradation of highly chlorinated
539 pesticide lindane in UV/peroxymonosulfate system. *Chem. Eng. J.* 318, 135-142.

540 Kim, M.H., Hwang, C.-H., Bin Kang, S., Kim, S., Park, S.W., Yun, Y.-S., Won, S.W., 2015. Removal of
541 hydrolyzed Reactive Black 5 from aqueous solution using a polyethylenimine-polyvinyl chloride
542 composite fiber. *Chem. Eng. J.* 280, 18-25.

543 Liang, C., Su, H.-W., 2009. Identification of Sulfate and Hydroxyl Radicals in Thermally Activated
544 Persulfate. *Ind. Eng. Chem. Res.* 48, 5558-5562.

545 Liang, C.J., Lee, I.L., Hsu, I.Y., Liang, C.P., Lin, Y.L., 2008. Persulfate oxidation of trichloroethylene
546 with and without iron activation in porous media. *Chemosphere* 70, 426-435.

547 Liu, X., Liu, Y., Lu, S., Wang, Z., Wang, Y., Zhang, G., Guo, X., Guo, W., Zhang, T., Xi, B., 2020.
548 Degradation difference of ofloxacin and levofloxacin by UV/H_2O_2 and UV/PS (persulfate):
549 Efficiency, factors and mechanism. *Chem. Eng. J.* 385.

550 Magazinovic, R.S., Nicholson, B.C., Mulcahy, D.E., Davey, D.E., 2004. Bromide levels in natural
551 waters: its relationship to levels of both chloride and total dissolved solids and the implications for
552 water treatment. *Chemosphere* 57, 329-335.

553 Masi, F., Rizzo, A., Bresciani, R., Martinuzzi, N., Wallace, S.D., Van Oirschot, D., Macor, F., Rossini,
554 T., Fornaroli, R., Mezzanotte, V., 2019. Lessons learnt from a pilot study on residual dye removal
555 by an aerated treatment wetland. *Sci. Total Environ.* 648, 144-152.

556 Nestmann, E.R., Douglas, G.R., Matula, T.I., Grant, C.E., Kowbel, D.J., 1979. Mutagenic activity of
557 rhodamine dyes and their impurities as detected by mutation induction in *Salmonella* and DNA
558 damage in Chinese hamster ovary cells. *Cancer Res.* 39, 4412-4417.

559 Neta, P., Huie, R.E., Ross, A.B., 1988. Rate constants for reactions of inorganic radicals in aqueous
560 solution. *J. Phys. Chem. Ref. Data* 17, 1027-1284.

561 Nihemaiti, M., Miklos, D.B., Huebner, U., Linden, K.G., Drewes, J.E., Croue, J.-P., 2018. Removal of
562 trace organic chemicals in wastewater effluent by UV/H₂O₂ and UV/PDS. *Water Res.* 145,
563 487-497.

564 Pouran, S.R., Aziz, A.R.A., Daud, W.M.A.W., 2015. Review on the main advances in photo-Fenton
565 oxidation system for recalcitrant wastewaters. *J. Ind. Eng. Chem.* 21, 53-69.

566 Rao, Y., Han, F., Chen, Q., Wang, D., Xue, D., Wang, H., Pu, S., 2019. Efficient degradation of
567 diclofenac by LaFeO₃-Catalyzed peroxymonosulfate oxidation-kinetics and toxicity assessment.
568 *Chemosphere* 218, 299-307.

569 Rao, Y.F., Xue, D., Pan, H.M., Feng, J.T., Li, Y.J., 2016. Degradation of ibuprofen by a synergistic
570 UV/Fe(III)/Oxone process. *Chem. Eng. J.* 283, 65-75.

571 Rasheed, T., Bilal, M., Iqbal, H.M.N., Shah, S.Z.H., Hu, H., Zhang, X., Zhou, Y., 2018.
572 TiO₂/UV-assisted rhodamine B degradation: putative pathway and identification of intermediates
573 by UPLC/MS. *Environmental Technology* 39, 1533-1543.

574 Rehman, F., Sayed, M., Khan, J.A., Shah, N.S., Khan, H.M., Dionysiou, D.D., 2018. Oxidative removal
575 of brilliant green by UV/S₂O₈²⁻, UV/HSO₅⁻ and UV/H₂O₂ processes in aqueous media: A
576 comparative study. *J. Hazard Mater.* 357, 506-514.

577 Semitsoglou-Tsiapou, S., Mous, A., Templeton, M.R., Graham, N.J.D., Leal, L.H., Kruithof, J.C., 2016.
578 The role of natural organic matter in nitrite formation by LP-UV/H₂O₂ treatment of nitrate-rich
579 water. *Water Res.* 106, 312-319.

580 Shankar, M.V., Nelieu, S., Kerhoas, L., Einhorn, J., 2007. Photo-induced degradation of diuron in
581 aqueous solution by nitrites and nitrates: Kinetics and pathways. *Chemosphere* 66, 767-774.

582 Shen, Y.-S., Lin, C.-C., 2003. The effect of pH on the decomposition of hydrophenols in aqueous
583 solutions by ultraviolet direct photolysis and the ultraviolet-hydrogen peroxide process. *Water
584 environment research : a research publication of the Water Environment Federation* 75, 54-60.

585 Stefan, M.I., 2017. *Advanced Oxidation Processes for Water Treatment: Fundamentals and
586 Applications.* IWA Publishing.

587 Su, S.N., Guo, W.L., Leng, Y.Q., Yi, C.L., Ma, Z.M., 2013. Heterogeneous activation of Oxone by
588 CoxFe₃xO₄ nanocatalysts for degradation of rhodamine B. *J. Hazard Mater.* 244, 736-742.

589 Tian, F.-X., Ma, S.-X., Xu, B., Hu, X.-J., Xing, H.-B., Liu, J., Wang, J., Li, Y.-Y., Wang, B., Jiang, X.,
590 2019. Photochemical degradation of iodate by UV/H₂O₂ process: Kinetics, parameters and
591 enhanced formation of iodo-trihalomethanes during chloramination. *Chemosphere* 221, 292-300.

592 Wang, C., Hofmann, M., Safari, A., Viöle, I., Andrews, S., Hofmann, R., 2019. Chlorine is preferred
593 over bisulfite for H₂O₂ quenching following UV-AOP drinking water treatment. *Water Res.* 165.

594 Wang, F.G., Wang, W.J., Yuan, S.J., Wang, W., Hu, Z.H., 2017. Comparison of UV/H₂O₂ and UV/PS
595 processes for the degradation of thiamphenicol in aqueous solution. *J. Photoch. Photobio. A* 348,
596 79-88.

597 Wang, P., Cheng, M., Zhang, Z., 2014. On different photodecomposition behaviors of rhodamine B on
598 laponite and montmorillonite clay under visible light irradiation. *Journal of Saudi Chemical*
599 *Society* 18, 308-316.

600 Wang, Y.R., Chu, W., 2011. Degradation of a xanthene dye by Fe(II)-mediated activation of Oxone
601 process. *J. Hazard Mater.* 186, 1455-1461.

602 Westerhoff, P., Mezyk, S.P., Cooper, W.J., Minakata, D., 2007. Electron pulse radiolysis determination
603 of hydroxyl radical rate constants with Suwannee river fulvic acid and other dissolved organic
604 matter isolates. *Environ. Sci. Technol.* 41, 4640-4646.

605 Xu, X.-R., Li, X.-Z., 2010. Degradation of azo dye Orange G in aqueous solutions by persulfate with
606 ferrous ion. *Sep. Purif. Technol.* 72, 105-111.

607 Zhang, T., Chen, Y., Wang, Y., Le Roux, J., Yang, Y., Croue, J.-P., 2014. Efficient Peroxydisulfate
608 Activation Process Not Relying on Sulfate Radical Generation for Water Pollutant Degradation.
609 *Environ. Sci. Technol.* 48, 5868-5875.

610 Zhang, T., Zhu, H., Croue, J.-P., 2013. Production of Sulfate Radical from Peroxymonosulfate Induced
611 by a Magnetically Separable CuFe₂O₄ Spinel in Water: Efficiency, Stability, and Mechanism.
612 *Environ. Sci. Technol.* 47, 2784-2791.

613 Zhang, Y., Luo, G., Wang, Q., Zhang, Y., Zhou, M., 2020. Kinetic study of the degradation of
614 rhodamine B using a flow-through UV/electro-Fenton process with the presence of
615 ethylenediaminetetraacetic acid. *Chemosphere* 240.

616 Zhang, Y., Xiao, Y., Zhong, Y., Lim, T.-T., 2019. Comparison of amoxicillin photodegradation in the
617 UV/H₂O₂ and UV/persulfate systems: Reaction kinetics, degradation pathways, and antibacterial
618 activity. *Chem. Eng. J.* 372, 420-428.

619 Zhao, X., Jiang, J., Pang, S., Guan, C., Li, J., Wang, Z., Ma, J., Luo, C., 2019. Degradation of
620 iopamidol by three UV-based oxidation processes: Kinetics, pathways, and formation of iodinated
621 disinfection byproducts. *Chemosphere* 221, 270-277.

622 Zhou, X., Zhou, Y., Liu, J., Song, S., Sun, J., Zhu, G., Gong, H., Wang, L., Wu, C., Li, M., 2019. Study
623 on the pollution characteristics and emission factors of PCDD/Fs from disperse dye production in
624 China. *Chemosphere* 228, 328-334.

625

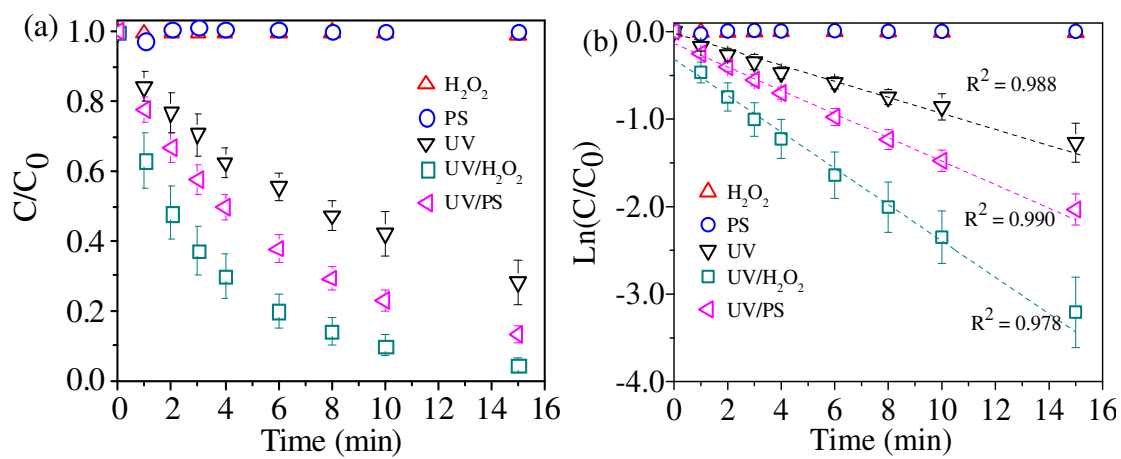


Fig. 1. (a) Relative degradation, and (b) pseudo-first-order kinetics of RhB in different oxidation

systems. ($[RhB]_0 = 10 \mu M$, $[H_2O_2]_0 = [PS]_0 = 50 \mu M$, $pH = 7$)

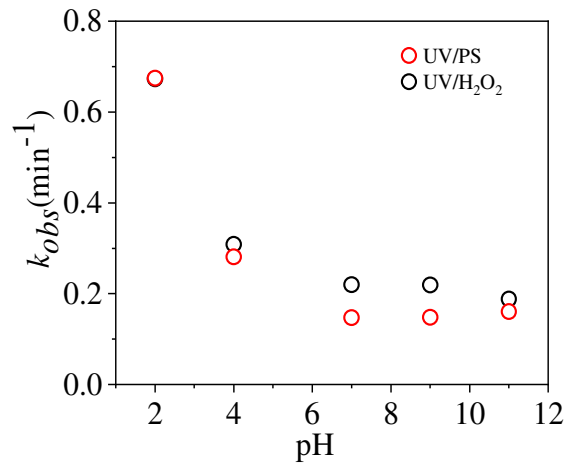


Fig. 2. Pseudo-first-order rate constant of RhB degradation under different initial solution pH in UV/ H_2O_2 and UV/PS systems. ($[\text{RhB}]_0 = 10 \mu\text{M}$, $[\text{H}_2\text{O}_2]_0 = [\text{PS}]_0 = 50 \mu\text{M}$, $\text{pH} = 7$)

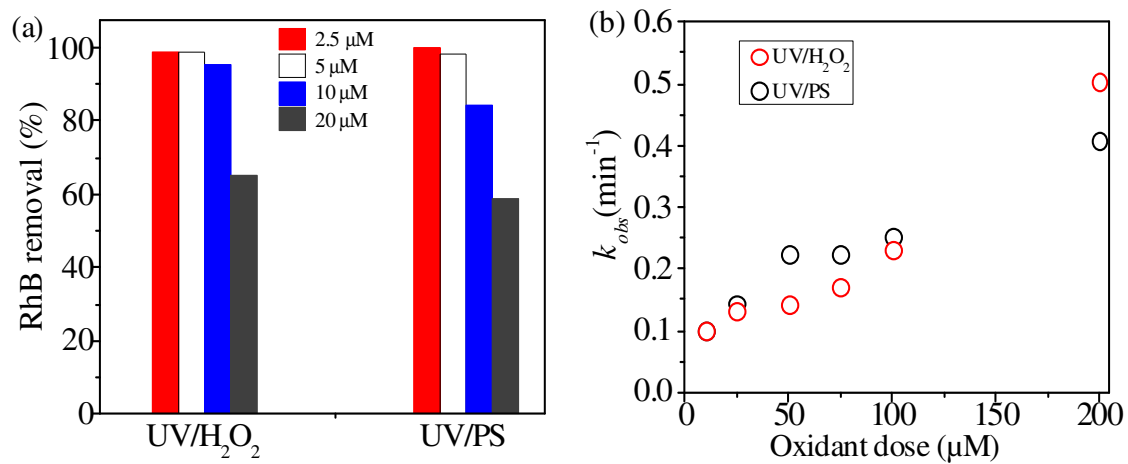


Fig. 3. RhB removal in UV/H₂O₂ and UV/PS systems under various (a) initial RhB concentration and (b)

varying oxidant dose. ($[H_2O_2]_0 = [PS]_0 = 50 \mu M$, pH = 7)

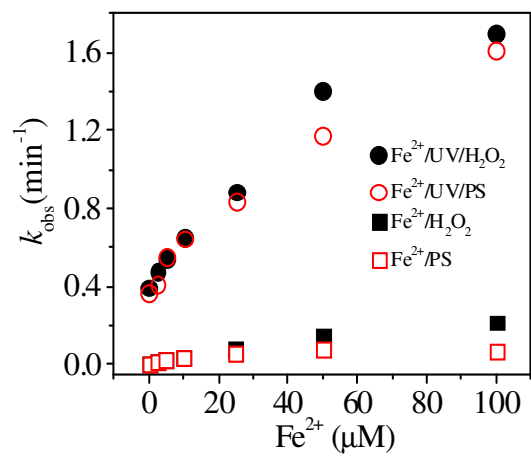


Fig. 4. Comparison of the pseudo-first-order rate constant (k_{obs}) of RhB degradation in different oxidation systems in the presence of Fe^{2+} as a transition metal activator. ($[\text{RhB}]_0 = 10 \mu\text{M}$, $[\text{H}_2\text{O}_2]_0 = [\text{PS}]_0 = 50 \mu\text{M}$, $\text{pH} = 3$)

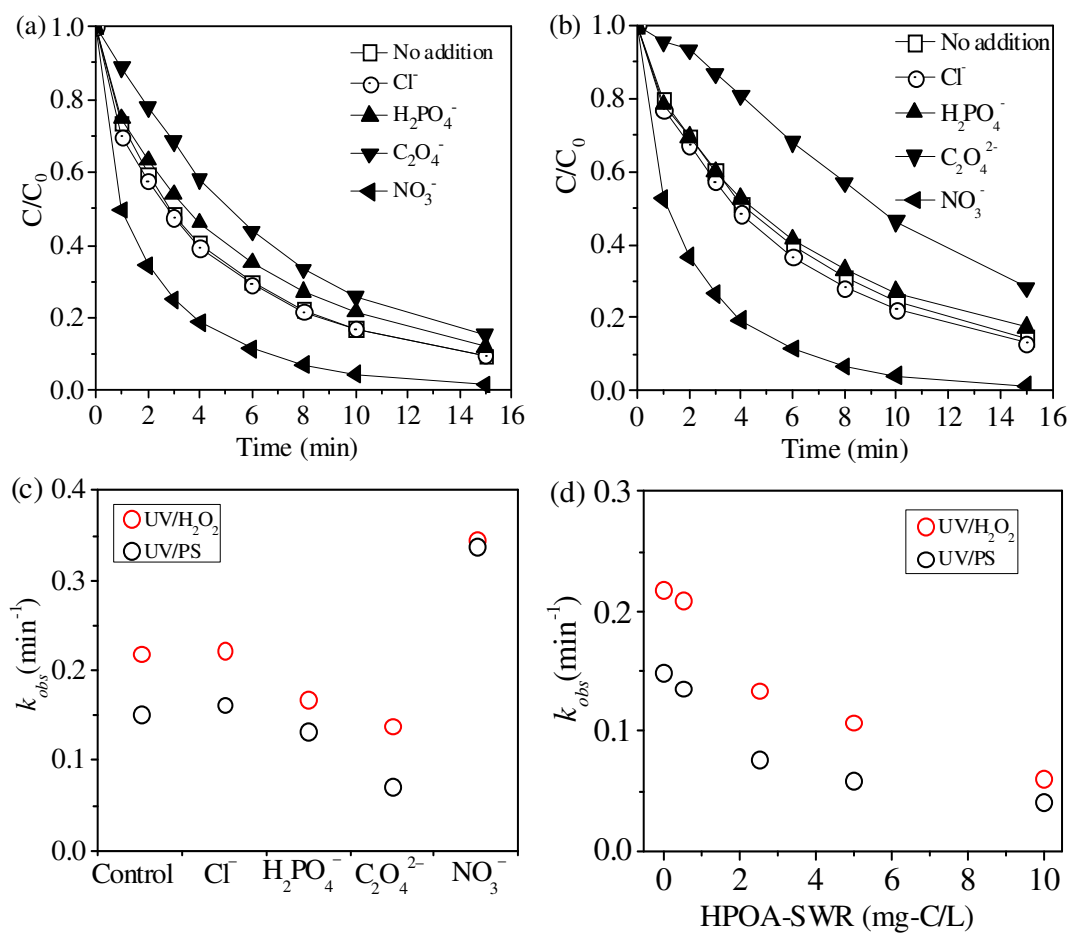


Fig. 5. Effect of different anions on the degradation of RhB in (a) UV/H₂O₂ and (b) UV/PS systems and

the pseudo-first-order rate constants of RhB degradation in the presence of different anions (c) and

varying concentrations of HPOA-SWR (d). ($[\text{RhB}]_0 = 10 \mu\text{M}$, $[\text{H}_2\text{O}_2]_0 = [\text{PS}]_0 = 50 \mu\text{M}$, $[\text{Cl}^-]_0 =$

$$[\text{H}_2\text{PO}_4^-]_0 = [\text{C}_2\text{O}_4^{2-}]_0 = [\text{NO}_3^-]_0 = 10 \text{ mM}, \text{pH}=7)$$

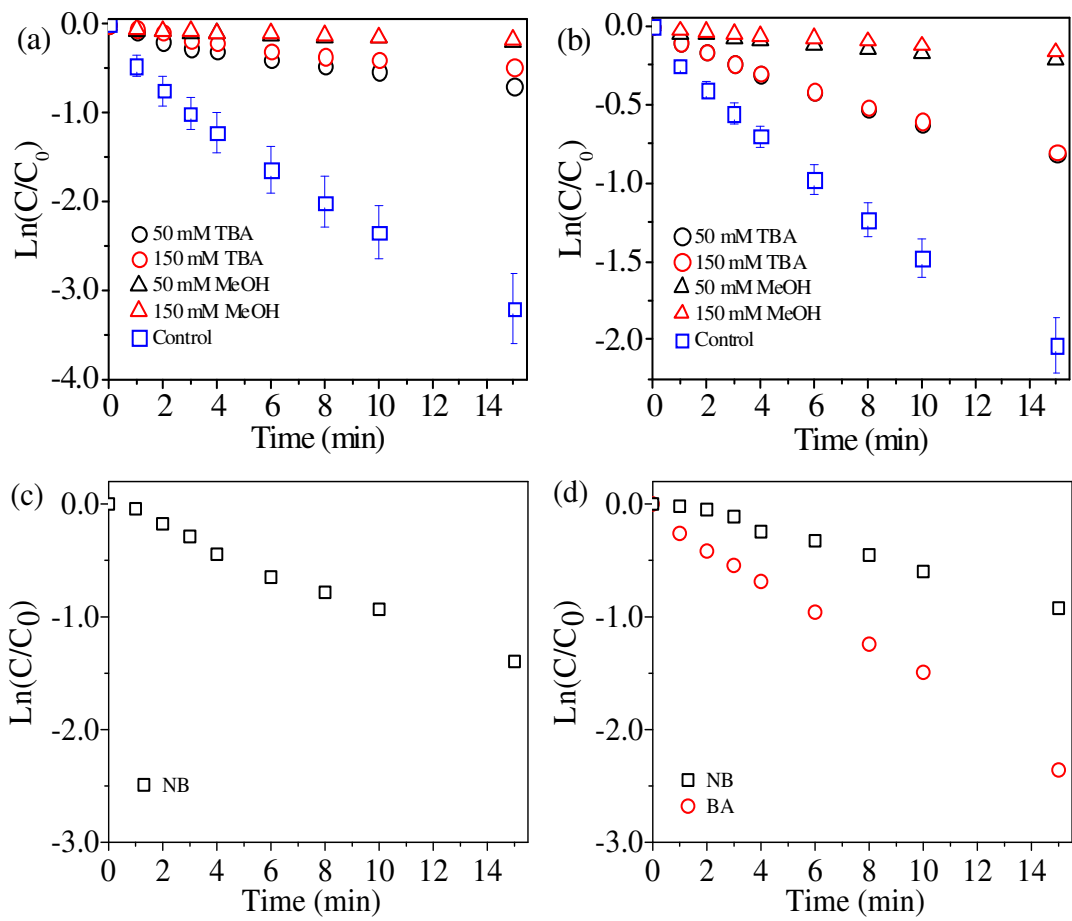


Fig. 6. The degradation of RhB in the presence of TBA or MeOH in (a) UV/H₂O₂ and (b) UV/PS systems, and the reaction kinetics of NB and BA degradation in the presence of 10 μ M RhB in (c) UV/H₂O₂ and (d) UV/PS systems. ($[\text{RhB}]_0 = 10 \mu\text{M}$, $[\text{H}_2\text{O}_2]_0 = [\text{PS}]_0 = 50 \mu\text{M}$, $[\text{NB}]_0 = [\text{BA}]_0 = 1 \mu\text{M}$, pH = 7)

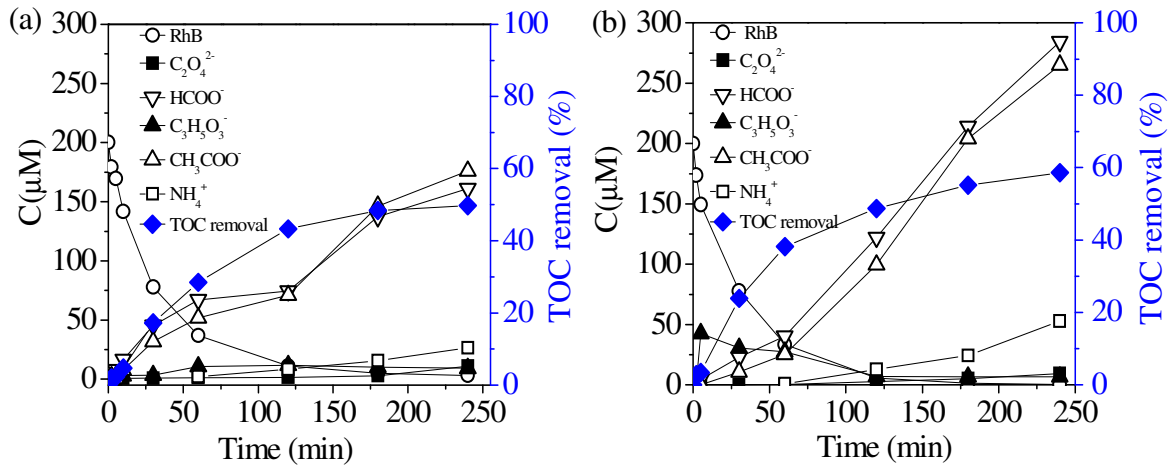


Fig. 7. Degradation and transformation of RhB and the subsequent formation of small molecular acids

and NH_4^+ in (a) UV/ H_2O_2 and (b) UV/PS systems. ($[\text{RhB}]_0 = 0.2 \text{ mM}$, $[\text{H}_2\text{O}_2]_0 = [\text{PS}]_0 = 1 \text{ mM}$, $\text{pH} = 7$)

Graphical Abstract

